Short communication: Runout of rock avalanches limited by basal friction but controlled by fragmentation

Øystein. T. Haug[1,2], Matthias Rosenau[1], Michael Rudolf[1], Karen Leever[1,3], and Onno Oncken[1]

[1]GFZ German Research Centre for Geosciences, Helmholtz Centre Potsdam, Telegrafenberg, 14473 Potsdam, Germany.
[2]Njord center, Department of Geosciences, University of Oslo, PO Box 1048, 0316 Oslo, Norway.
[3]Van Hall Larenstein University of Applied Sciences, Larensteinselaan 26a, 6882 Velp, The Netherlands.

Correspondence: Matthias Rosenau (rosen@gfz-potsdam.de)

Abstract. Rock avalanches [c1]produce exceptionally long [c2]runouts that correlate with their [c3]rock volume. This relationship has been attributed to [c4]the size-dependent dynamic lowering of the effective basal friction. However, [c5]it has also been observed that runouts [c6]of rock avalanches with similar volumes can span several orders of [c7]magnitude, suggesting additional controlling factors. Here, we [c8]analyze analog models of rock [c9]avalanches, with the experiments designed to test the role of dynamic fragmentation. We show that for a fixed low basal friction, the runout of experimental rock avalanches varies over two orders of magnitude and is determined by their degree of fragmentation while the basal friction acts only as an upper [c10]limit on runout. We interpret the runout's dependence on fragmentation to be controlled by the competition between mobility enhancing spreading and [c11]energy-consuming fragmentation limited by basal friction. We formalize this competition into a scaling law based on energy conservation which shows that [c12]the variation in the degree of fragmentation can [c13]contribute to the large variation in runout of rock avalanches seen in nature.

[c1]*MRo*: display
[c2]*MRo*: runouts, which are found to
[c3]*MRo*: volume and
[c4]*MRo*: size dependent
[c5]*MRo*: even for similar volumes,
[c6]*MRo*: are seen to
[c7]*MRo*: magnitude
[c8]*MRo*: here analyse experiments with analogue
[c9]*MRo*: avalanches aimed at testing
[c10]*MRo*: limiter.
[c11]*MRo*: energy consuming internal
[c12]*MRo*: *Text added.*
[c13]*MRo*: explain

1 Introduction

With volumes larger than [c14]10^9 m^3, and speeds reported at over 150 km/h [c15](Campbell, 1989) and possibly up to 100m/s (Legros, 2002), the destructive power of rock avalanches is unprecedented. They are exceptional hazards produced when very large rockslides disintegrate during transport (Hungr et al., 2013). The travel distance of the deposit front, or runout, is an important measure for [c16]hazard assessment (Vaunat and Leroueil, 2002) and is generally found to bemore than ten times longer than [c17]the fall height (Hsü, 1975). This suggests low effective basal [c18]friction μ_{eff}, which is usually attributed to [c19]various dynamic weakening processes (e.g. Kent, 1966; Shreve, 1968; Hsü, 1975; Melosh, 1979; Campbell, 1989; Pudasaini and Miller, 2013; Legros, 2002; Lucas et al., 2014; Wang et al., 2017) or [c20]additional basal erosion processes (e.g. Hungr and Evans, 2004; Pudasaini and Fischer, 2020).

Field observations of the displacement of rock avalanches [c1]are typically given by the ratio of vertical (H) and horizontal (L) distance from the deposit's front to the top of the main scarp. The resulting ratio [c2]

$$\mu_{apparent} = \frac{H}{L} \quad (1)$$

is known as the Heim's ratio (Heim, 1882, as cited in Hsü, 1975) and serves as a proxy for μ_{eff} when called the [c3]"apparent" coefficient of friction (Manzella and Labiouse, 2012). One of the best established, but perhaps least understood observations of rock avalanches, is the dependence of the Heim's ratio on volume: rockslides below a size of approximately 10^6 m^3 all have a relatively constant Heim's ratio of ∼0.4-0.7, but for larger rockslides [c4]Heim's ratio decreases with volume, reaching values <0.1 for volumes larger than 10^9 m^3 [c5](Pudasaini and Miller, 2013; Lucas et al., 2014). This suggests a [c6]scale-dependent mechanism of decreasing apparent friction with volume that [c7]becomes dominant at large volumes (Davies and McSaveney, 1999). [c8]Analytical modeling and numerical simulation involving lubrication mechanisms by [c9]Pudasaini and Miller (2013) and Lucas et al. (2014) [c10]provided mechanical explanations for this [c11]observation. Importantly, [c12]however, even [c13]within

[c14]*MRo*: 10^6 m^3,
[c15]*MRo*: (Campbell, 1989),
[c16]*MRo*: their
[c17]*MRo*: their
[c18]*MRo*: frictions
[c19]*MRo*: either a reduced normal stress at the base (e.g. Kent, 1966; Shreve, 1968; Hsü, 1975; Melosh, 1979; Campbell, 1989)
[c20]*MRo*: a velocity dependent decrease of the friction coefficient (e.g. Wang et al., 2017).
[c1]*MRo*: is
[c2]*MaRo*: ~~$\mu_{ap} = \frac{H}{L}$~~
[c3]*MRo*: apparent
[c4]*MRo*: it
[c5]*MRo*: (Lucas et al., 2014).
[c6]*MRo*: scale dependent
[c7]*MRo*: is only relevant for
[c8]*MRo*: Whether the effective friction itself depends on size is uncertain, though analysis
[c9]*MRo*: *Text added.*
[c10]*MRo*: suggests that
[c11]*MRo*: is the case.
[c12]*MRo*: *Text added.*
[c13]*MRo*: when similar volumes are considered,

a narrow range of volumes, runouts are seen to span [c14]orders of magnitude suggesting additional controlling [c15]factors on runout that are insensitive to size. Runout variability lies in part [c16]also in the fact that the runout is defined by the front of the deposits, and therefore contains the combined effect of both translation and spreading of the rock mass. The additional travel distance caused by spreading can have a profound effect on the runout (Staron and Lajeunesse, 2009), especially if the effective basal friction is low.

[c1]Recently, the process of dynamic fragmentation [c2]has received increased attention [c3]from the reserach community, and [c4]much progress [c5]has been made in our understanding of its role in the dynamics of rock avalanches [c6](Locat et al., 2006; Imre et al., 2010; Bowman et al., 2012; Pudasaini and Miller, 2013; De Blasio and Crosta, 2015; Haug et al., 2016; Zhao et al., 2017, 2018; Lin et al., 2020; Gao et al., 2020; Knapp and Krautblatter, 2020). Firstly, one may expect that the finer the material, the more flow-like the behavior, increasing its mobility and allowing the rock mass to spread more easily (Locat et al., 2006; Wang et al., 2017; Zhao et al., 2018). Secondly, models of fragmenting rockslides suggest that dynamic fragmentation actively increases the spreading (Bowman et al., 2012; De Blasio and Crosta, 2015; Lin et al., 2020). However, fragmentation has also been shown to consume energy (Haug et al., 2016; Zhao et al., 2017; Lin et al., 2020), potentially at a cost to the runout length. Clearly, [c7]understanding the integrated effect of fragmentation on the runout dynamics of rock avalanches [c8]requires more analysis.

[c9]To study the effects of friction and fragmentation on rock avalanche dynamics, we here [c10]analyze analog models of dynamically fragmenting rock slides. [c11]We assume that there exists some mechanism [c12](or a set of mechanisms) that causes a [c13]low effective coefficient of basal friction [c14]which we set to 0.15-0.2 in our models. To isolate the scale-independent effect of fragmentation we keep [c15]both the volume and friction within a narrow range in our [c16]models compared to the nature. Note, this approach explicitely excludes dynamic weakening mechanisms that are suspected in natural prototypes. Specifically, our models do not include fluids and frictional heating is insignificant such that [c17]lubrication mechanisms (e.g.

[c14]*MRo*: several oders
[c15]*MRo*: factors. The uncertainty
[c16]*MRo*: *Text added.*
[c1]*MRo*: Only recently,
[c2]*MRo*: *Text added.*
[c3]*MRo*: *Text added.*
[c4]*MRo*: *Text added.*
[c5]*MRo*: occurs
[c6]*MRo*: (Locat et al., 2006; Bowman et al., 2012; De Blasio and Crosta, 2015; Haug et al., 2016; Zhao et al., 2017, 2018; Lin et al., 2020; Gao et al., 2020; Knapp and Krautblatter, 2020).
[c7]*MRo*: *Text added.*
[c8]*MRo*: remains to be specified.
[c9]*MRo*: In order to isolate
[c10]*MRo*: analyse analogue
[c11]*MRo*: Weassume
[c12]*MRo*: *Text added.*
[c13]*MRo*: low, but constant
[c14]*MRo*: and
[c15]*MRo*: it constant
[c16]*MRo*: model. This entails
[c17]*MRo*: any experimentally

Pudasaini and Miller, 2013; Lucas et al., 2014) do not play a role. Granular pressurization (e.g. Imre et al., 2010) is also not considered significant in our experiments because of the low energy involved. Other potentially important mechanisms like bedrock erosion (e.g. Hungr and Evans, 2004; Pudasaini and Fischer, 2020) are excluded here for simplicity. The experimental design, therefore, means that the observed variation in Heim's ratio is due to [c18]fragmentation and dry friction. We describe the dependence observed between the runout and the degree of fragmentation in the form of a scaling law. Finally, we compare our experimental results to a set of natural data and discuss their relevance to natural systems. All data underlying this study as well as additional relevant data are published open access in Haug et al. (2020).

2 Experimental methods

In the experiments, originally documented in Haug et al. (2016), a block of height h and length l_0 (width = l_0) of rock [c1]analog material is gravitationally accelerated down a plate held at an angle of 45° to the horizontal (Figure 1). After 1 m of travel, the sample impacts a horizontal plate causing it to fragment. Once the sample fragments have [c2]slid onto the horizontal [c3]plane, they spread and decelerate due to [c4]the internal and basal frictional [c5]interaction, before finally [c6]coming to rest. We use silicate glass as our substrate, on which the basal friction coefficient is ca. [c7]0.15-0.20 (Haug et al., 2016) - similar to the lowermost values found in natural prototypes (Pudasaini and Miller, 2013; Lucas et al., 2014). The [c8]analog rock material is a cemented fluvial quartz sand. The sand is cemented by mixing it with water and gypsum or potato [c9]starch and is left to set for 2 days (for gypsum cement) or heated for 15 minutes in a 900 W microwave (for potato starch cement). The cohesion of the material can be controlled by the type and [c10]amount of cement added to the mixture, allowing control [c11]of the strength of the material over several orders of magnitude. The internal friction coefficient relevant for fragmenting intact material is 0.7 and reduces to 0.6 when fragments interact (see Haug et al., 2014, 2016, for details on the experimental setup).

[c12]

The three main observables from the experiments are: (i) the degree of fragmentation (m_c), (ii) the Heim's ratio [c13](H/L), and (iii) the normalized deposit length (L_{spread}/H). We characterize the degree of fragmentation through the total mass of the sample divided by the mass of the largest fragment ($m_c =$ [c14]M/m_{max}). We choose this rather simple parameter, which

---

[c18]*MRo*: fragmentation.
[c1]*MRo*: analogue
[c2]*MRo*: slide
[c3]*MRo*: plate, the fragments spread,
[c4]*MRo*: *Text added.*
[c5]*MRo*: contact and
[c6]*MRo*: come
[c7]*MRo*: 0.15 (Haug et al., 2016).
[c8]*MRo*: analogue
[c9]*MRo*: starch,
[c10]*MRo*: the
[c11]*MRo*: on
[c12]*MRo*: Sketch of the slope geometry of experiments and various length measurements (modified after Haug et al. (2016))
[c13]*MRo*: (H/L)
[c14]*MRo*: M/m_{max}), justification of

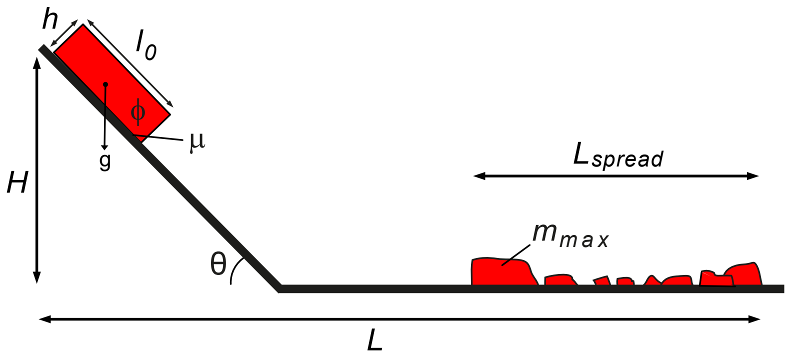

Figure 1. Sketch of the slope geometry of experiments, relevant parameters, and length scales (modified after Haug et al. (2016))

[c15]has been validated and benchmarked against breakage parameters used by previous studies in [c16]Haug et al. (2016), as a tradeoff between capturing the process accurately in models and the accessibility of the [c17]equivalent information in nature. To define L_{spread}, we consider the mass-weighted average position of the most [c18]proximal and distal 5 % of [c19]the total mass. This defines a [c20]rim which is a more robust runout estimate than using [c21]single fragment [c22]positions as used by [c23]Haug et al. (2016) and is at the same time accessible both experimentally and empirically. We normalize L_{spread} by fall height H in order to have a parameter describing the conversion of potential energy into spreading equivalent to Heim's ratio.

The experimental data [c1]analyzed here [c2]are coming from two series of experiments with varying degree of fragmentation: (i) one series of experiments where the [c3]thickness to length ratio [c4](h/l_0) of the samples [c5]has been varied [c6]between 0.033 and 0.49 (corresponding to a one order of magnitude range in volume) while keeping the cohesion [c7](C) constant at [c8]14 kPa. (ii) one series of experiments where the cohesion of the material is varied [c9]between 4 [c10]and 350 kPa while keeping the thickness to length ratio constant at [c11]0.13. In both series of experiments, the fall height (H) is kept constant at 0.71 m.

[c15]*MRo*: can be found
[c16]*MRo*: Haug et al. (2016). The front (and back)
[c17]*MRo*: deposit is determined by
[c18]*MRo*: *Text added.*
[c19]*MRo*: *Text added.*
[c20]*MRo*: frontal
[c21]*MRo*: the foremost
[c22]*MRo*: position,
[c23]*MRo*: Haug et al. (2016).
[c1]*MRo*: analysed
[c2]*MRo*: stem
[c3]*MRo*: the
[c4]*MRo*: $(h/l_0 = 0.033 - 0.49)$
[c5]*MRo*: is
[c6]*MRo*: *Text added.*
[c7]*MRo*: *Text added.*
[c8]*MRo*: $C = 14$
[c9]*MRo*: $(C =$
[c10]*MRo*: - 350 kPa)
[c11]*MRo*: $h/l_0 = 0.13$.

Interested readers are referred to Haug et al. (2016) for details on the effect of cohesion and geometry on the degree of fragmentation. Additionally, two new experiments were performed to study [c12]the moment of fragmentation at high temporal resolution. For these experiments, the fragmentation of two samples with different cohesions but equal geometry ($C = 4$ and 40 kPa, $h/l_0 = 0.13$) is considered. These two experiments have a fall height of 0.35 m, and data is captured by a camera with a frame rate of 500 Hz (see Haug et al., 2020, for movies of these experiments).Combining these sets of data from various experiments allows for covering a wide enough parameter space for the analysis in this study.

3 Results and discussion

3.1 Experimental observations and interpretation

[c1]Figure 2 presents snapshots from two representative experiments, one with an intermediate strong sample and one with [c2]a low strength sample, illustrating the process of [c3]fragmentation. The [c4]stronger sample (Figure 2a) is observed to fragment less than the weaker one (Figure 2b). Threafter, fragments of [c5]the [c6]stronger sample spread with limited interaction while the [c7]fragments from the weaker sample collide and/or slide next to [c8]each other and deposition starts relatively early. We infer, at first order, that while mobility generally increases with fragmentation, [c9]a [c10]higher amount of [c11]internal deformation is [c12]experienced along with increased fragmentation and increased deposition.

[c13]Switched Figure 2 and 3

[c14]To quantitatively analyze the [c15]experiments, we focus on the [c16]correlation between runout and fragmentation and neglect all other parameters. This is [c17]justified by the [c18]collapse of [c19]experimental and natural data when plotting Heim's ratio against fragmentation in Figure 3a. Qualitatively, Heim's ratio decreases rapidly for low to [c20]intermediate degrees of fragmentation,

---

[c12]*MRo*: in detail
[c1]*MRo*: The Heim's ratio for experiments
[c2]*MRo*: different degrees
[c3]*MRo*: fragmentation (m_c) is plotted in Figure 2a.
[c4]*MRo*: two series
[c5]*MRo*: experiments follow
[c6]*MRo*: same trend (Haug et al., 2016), and no distinction is made between them in this figure. It shows that
[c7]*MRo*: Heim's ratio decreases rapidly for low
[c8]*MRo*: intermediate degrees of
[c9]*MRo*: reaching
[c10]*MRo*: minimum at $m_c \approx 5$ of about 0.2. With further increase
[c11]*MRo*: fragmentation a gentle increase in the Heim's ratio is observed. A similar behavior
[c12]*MRo*: observed for the length of the deposits (Figure 2b), which increase until $m_c \approx 5$ before it decreases for higher values.
[c13]*MRo*: *Text added.*
[c14]*MRo*: Figure 3 presents snapshots from
[c15]*MRo*: two additional experiments. As expected,
[c16]*MRo*: sample with the highest cohesion (Figure 3a)
[c17]*MRo*: observed to fragment less than the one with a lower cohesion (Figure 3b). Accordingly,
[c18]*MRo*: fragments
[c19]*MRo*: the stronger sample spread with limited interaction while the fragments from the weaker sample collide and/or slide next
[c20]*MRo*: each other. As a consequence,

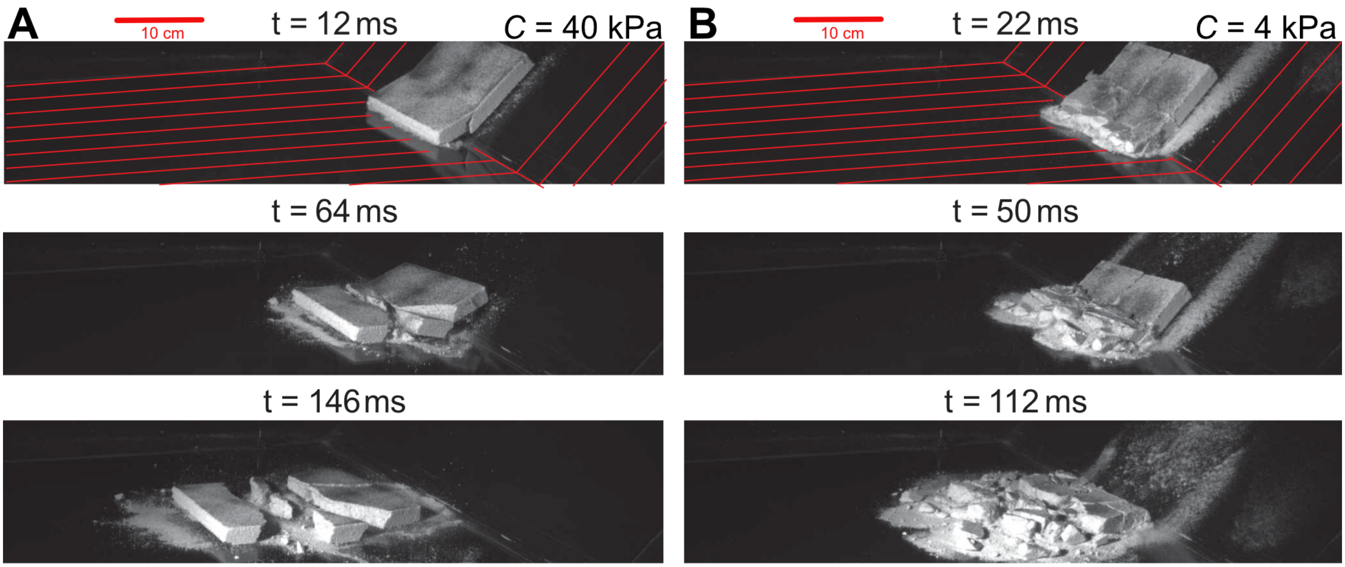

Figure 2. Snapshots from the experiments: (A) intermediate strength sample ($C = 40\,\text{kPa}$) and (B) low strength sample ($C = 4\,\text{kPa}$).The red lines in the upper images indicate the geometry of the basal plates. Images are chosen to represent similar travel distances in (A) and (B). The time given above each image reflects the time since the first impact. The samples have dimensions 15x15x2 cm. Note that the stronger sample (a) breaks apart into six large fragments with a limited amount of fine material produced and moves apart with little interaction after breaking. In contrast, the weaker sample fragments into many small pieces with a large fraction of fine material causing frictional interaction and that deposits relatively early. Movies of the experiments are available in Haug et al. (2020).

reaching a [c21]minimum at $m_c \approx 5$ of about 0.2 and increases again slightly for higher [c22]degrees of [c23]fragmentation. A similar relation is [c24]observed between the length of the deposits (Figure 3b), which increases with [c25]fragmentation until $m_c \approx 5$ and slightly decreases beyond.

The rapidly decreasing [c1]Heim's ratio for $m_c < 5$ observed in [c2]Figure 3a is likely [c3]linked to the increased spreading with fragmentation [c4]seen in Figure 3b. A similar result was also obtained by previous [c5]analog experiments (Bowman et al., 2012; Haug et al., 2016) as well as numerical models (De Blasio and Crosta, 2015; Zhao et al., 2017). However, here we show that the Heim's ratio is not simply decreasing with the degree of fragmentation, but that it displays an optimum for $m_c \approx 5$. Importantly, the lowest apparent basal friction, equivalent to the lowest Heim's ratio, is close to the implemented basal

[c21]*MRo*: *Text added.*
[c22]*MRo*: amount
[c23]*MRo*: internal deformation
[c24]*MRo*: experienced
[c25]*MRo*: increased fragmentation.
[c1]*MRo*: Heims's
[c2]*MRo*: Figure 2a
[c3]*MRo*: caused by
[c4]*MRo*: (Figure 2b).
[c5]*MRo*: analogue

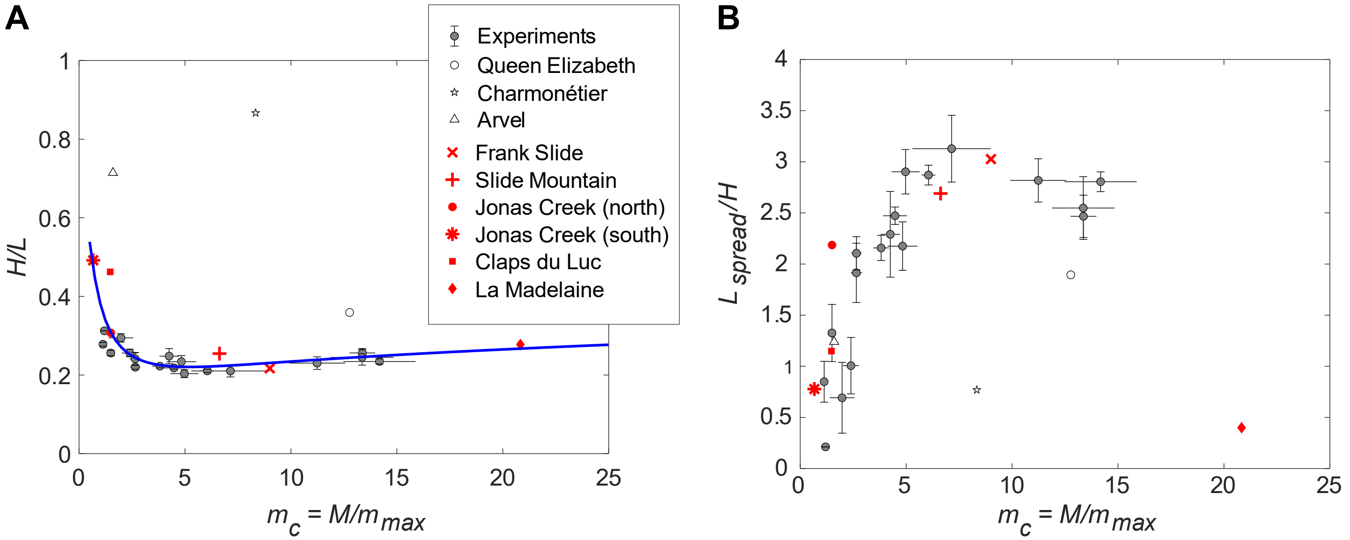

Figure 3. Heim's ratio and deposit length of experiments (this study) and natural rock avalanches (from Locat et al., 2006). (A) The Heim's ratio of the analog experiments (grey) and from the rock avalanches (red = selected set, open = discarded). The blue line represents the best fit of Equation 8 to experimental and natural data with parameters $\alpha = -1.0$, $\beta = 1.5$, $\gamma = 0.11$. (B) The deposit's lengths. In both panels, the grey circles represent the average value of a set of 4-15 experiments and the error bars give the standard error of the set. Note the opposite trends of the two curves suggesting an intrinsic relationship between spreading and runout.

friction (i.e. friction coefficient of [c6]0.15-0.2 between samples and glass). Therefore, all processes operating in our models (e.g. fragmentation, internal friction between [c7]fragments, deposition) tend to consume energy and thereby reduce runout from its optimum (Haug et al., 2016). Considering the increased internal deformation observed with the degree of fragmentation [c8](Figure 2), the reduction of runout [c9]and spreading for $m_c > 5$ appears to be the result of the increased energy dissipation through internal [c10]friction within the rock mass as well as an increase in basal friction as the sliding surface becomes rougher due to syn-sliding deposition (e.g. Pudasaini and Fischer, 2020). A loss of mass and therefore momentum due to deposition may additionally result in deceleration and reduced runout as a function of m_c (e.g. Pudasaini and Fischer, 2020). Consequently, the minimum of the Heim's ratio observed in [c11]Figure 3a appears as the result of a competition between [c12]the spreading [c13]enhancing mobility and [c14]the energy-consuming fragmentation process.

[c6]*MRo*: 0.15
[c7]*MRo*: fragments)
[c8]*MRo*: (Figure 3),
[c9]*MRo*: with
[c10]*MRo*: friction.
[c11]*MRo*: Figure 2a is
[c12]*MRo*: *Text added.*
[c13]*MRo*: *Text added.*
[c14]*MRo*: internal friction.

3.2 A scaling law for runout

The interplay between fragmentation and friction [c1]in a dry environment can be formalized into a scaling law by considering the conservation of energy. Generally, the conservation of energy of a sliding mass M requires that

$$MgH = \mu M g L_p + W \tag{2}$$

where g is the gravitational acceleration, H is the vertical fall height, L_p is the entire travel path of the slide and W is the sum of any other energy dissipating terms. Here, we have assumed a Coulomb friction coefficient μ at the base.

For the geometry of our experimental setup [c2](see Figure A1), and also roughly for the set of selected rock avalanches, the L_p can be expressed in terms of the horizontal runout L as [c3]

$$L_p = L + L_s(1-\cos\theta) - \frac{1}{2}l_0 - \frac{1}{2}L_{spread} \tag{3}$$

where L_s is the length and θ the angle of the slope, and l_0 is the initial length of the slide. It is assumed that the additional travel length due to spreading is equal to half the deposit length (L_{spread}). Since l_0 is expected to be very small compared to the other terms, it is neglected in [c4]further analysis. Inserting [c5]Equation 3 into Equation 2 and solving for L gives [c6]

$$L = \frac{H}{\mu} - L_s(1-\cos\theta) + \frac{1}{2}L_{spread} - \frac{1}{\mu M g}W \tag{4}$$

where it is emphasized that both L_{spread} and W [c7]are expected to be functions of the basal friction, μ, internal friction, ϕ, the degree of fragmentation, m_c, as well as a possible non-linear dependence between L_{spread} and W. [c8]Rearranging Equation 4 yields the Heim's ratio [c9]in the form of [c10]

$$\frac{H}{L} = \mu\left(1 - \frac{\mu}{\sin\theta}(1-\cos\theta) + \frac{\mu}{2H}L_{spread} - \frac{1}{MgH}W\right)^{-1}. \tag{5}$$

A direct determination of the two last terms in Equation 5 is [c11]difficult. [c12]However, based on the shape of [c13]the function of both the [c14]Heim's ratio and the L_{spread} plotted in [c15]Figure 3, it appears that it can be reasonably described by an exponential

---

[c1] *MRo*: *Text added.*

[c2] *MRo*: (i.e. Figure 1),

[c3] *MRo*: $L_p = L + L_s(1-\cos\theta) - \frac{1}{2}l_0\cos\theta - \frac{1}{2}L_{spread}$

[c4] *MRo*: the

[c5] *MRo*: this expression

[c6] *MRo*: $L = \frac{H}{\mu} - L_s(1-\cos\theta) + \frac{1}{2}L_{spread}(\mu,\phi,m_c) - \frac{1}{\mu M g}W(\mu,\phi,m_c)$

[c7] *MRo*: is

[c8] *MRo*: With this expression for the runout,

[c9] *MRo*: is

[c10] *MRo*: $\frac{H}{L} = \mu\left(1 - \frac{\mu}{\sin\theta}(1-\cos\theta) + \frac{\mu}{2H}L_{spread}(\mu,\phi,m_c) - \frac{1}{MgH}W(\mu,\phi,m_c)\right)^{-1}$

[c11] *MRo*: difficult, however, the experimental work by Haug et al. (2016), suggests that W/Mgh can be described with a logarithmic function of m_c. Additionally,

[c12] *MRo*: *Text added.*

[c13] *MRo*: *Text added.*

[c14] *MRo*: Heim'

[c15] *MRo*: Figure 2,

function of [c16]m_c: [c17]

$$\frac{\mu}{2H}L_{spread} = \alpha e^{-m_c/\beta}. \tag{6}$$

[c1]Additionally, the [c2]experimental work by Haug et al. (2016) suggests that dissipative energy loss through fragmentation increases less for higher degrees of fragmentation and therefore can be [c3]described with a logarithmic function of m_c: [c4]

$$\frac{1}{MgH}W = \gamma log(m_c). \tag{7}$$

Using these approximations, Heim's ratio can be expressed as [c5]

$$\frac{H}{L} = \mu\left(1 - \frac{\mu}{\sin\theta}(1-\cos\theta) + \alpha e^{-m_c/\beta} - \gamma log(m_c)\right)^{-1} \tag{8}$$

where α, β, and γ are constants to be empirically determined.

[c6]This equation describes the competition between spreading (proportional to $e^{-m_c/\beta}$) and the increasing energy dissipation (proportional to $\log(m_c)$) with m_c and its relation to friction. A best fit of this function to the natural and experimental data is presented in Figure 3a (blue line), where $\alpha = -1.0$, $\beta = 1.5$, $\gamma = 0.11$. A fit constrained only the experimental data yields very similar results ($\alpha = -0.68$, $\beta = 2.0$, $\gamma = 0.11$, see Figure B1). This suggests spreading dominates runout for low degrees of fragmentation (i.e. $m_c < 5$), but has little effect at high degrees of fragmentation as the exponential term approaches zero. At high degrees of fragmentation, the energy dissipation related to fragmentation, therefore, becomes increasingly relevant in controlling runout. At $m_c \approx 5$, i.e. when about 80-85 % of the volume is fragmented, a state of optimal mobility is reached with a Heim's ratio limited by the basal friction coefficient suggesting that energy is consumed mainly by basal friction, which then is the limiting factor for runout.

[c16]*MRo*: m_c. This leads to the approximation that

[c17]*MRo*: ~~$\frac{L_{spread}(\mu,\phi,m_c)}{2H} - \frac{W(\mu,\phi,m_c)}{MgH} = -\alpha log(m_c) - \beta e^{-m_c/\gamma}$~~

[c1]*MRo*: such that

[c2]*MRo*: Heim's ratio

[c3]*MRo*: expressed as

[c4]*MRo*: *Text added.*

[c5]*MRo*: ~~$\frac{H}{L} = \mu\left(1 + \frac{\mu}{\sin\theta}(1-\cos\theta) - \alpha log(m_c) - \beta e^{-m_c/\gamma}\right)^{-1}$~~

[c6]*MRo*: This equation describes the competition between spreading ($\beta e^{-m_c/\gamma}$) and the increasing energy dissipation ($\alpha log(m_c)$) with m_c and its relation to friction. A best fit of this function to the natural and experimental data is presented in Figure 2a (blue line), where $\alpha = 0.11$, $\beta = 1.0$ and $\gamma = 1.5$. A fit to the experimental data only yields very similar results ($\alpha = 0.11$, $\beta = 0.68$ and $\gamma = 2.0$, see Figure A1). This suggests spreading dominates for low degrees of fragmentation (i.e. $m_c < 5$), but has little effect at high degrees of fragmentation as the term $\beta e^{-m_c/\gamma}$ approaches zero. At high degrees of fragmentation, the energy dissipation related to fragmentation therefore becomes increasingly relevant. At $m_c = 5$ a minimum is reached in which energy is consumed mainly by basal friction.

3.3 Application to a natural data set

We compare our experimental results [c7]in Figure 3 with data from nine rock avalanches reported by [c8]Locat et al. (2006) that show no clear volume dependence of runout. This [c9]feature makes this data set ideal [c10]for testing whether a scale-independent process is operating besides dynamic basal weakening. However, not all the rock avalanches reported in (Locat et al., 2006) are comparable to our experimental setup [c11]concerning material properties and geometries (Figure 1). Based on slope geometry, the Queen Elizabeth slide is discarded because of its run-up on the opposite valley wall. Also discarded is the Charmonétier slide because of the sudden [c12]free-fall stage at the end of its transport. Additionally, the Arvel slide was observed to bulldoze soft material in front of it, and such complexities are not considered in our models so this one is also neglected. [c13]Note that in all three discarded cases, the late-stage processes tend to increase the expected Heim's ratio and they consistently plot above the trend of the other data in Figure 3b.

[c1]Figure 3 displays remarkably similar trends between the experimental and the selected natural data that all follow the proposed scaling law. The data points from Jonas Creek (north) and Clapse du Luc are observed to extend the trend from the experiments to higher Heim's [c2]ratios for low degrees of fragmentations while La Madelaine slide is observed to extend the trend of the experimental results of Heim's ratio to higher degrees of fragmentation [c3](Figure 3a). Its low spreading value [c4](Figure 3b) suggests that the reduction of spreading indicated by the experiments for $m_c > 5$ continues for even higher degrees of fragmentation. The agreement between these slide deposit lengths and the extrapolation of the experimental trend through Equation 8 [c5](Figure 3b) supports the validity [c6]of our proposed scaling law. The Heim's ratios of the neglected slides are all, as expected, higher than the selected data set for their respective degrees of fragmentation, illustrating the importance of topography (e.g. opposite valley wall) and processes such as bulldozing.

The similarity seen between experimental and natural data suggests [c7]some universality [c8]concerning the empirical [c9]constants. Moreover, the similarity suggests that the rock avalanches considered here all have a close to constant effective [c10]basal friction

[c7] *MRo*: (Figure 2)
[c8] *MRo*: Locat et al. (2006), which
[c9] *MRo*: *Text added.*
[c10] *MRo*: to test
[c11] *MRo*: by means of
[c12] *MRo*: free fall
[c13] *MRo*: *Text added.*
[c1] *MRo*: Figure 2
[c2] *MRo*: ratio
[c3] *MRo*: (Figure 2a).
[c4] *MRo*: (Figure 2b)
[c5] *MRo*: (Figure 2b) makes us confident about
[c6] *MRo*: and predictive power
[c7] *MRo*: *Text added.*
[c8] *MRo*: with respect to
[c9] *MRo*: constants and
[c10] *MRo*: *Text added.*

of about [c11]0.15-0.2. This implies [c12]that over [c13]the range of two orders of magnitude (from $2 \cdot 10^6$ to $90 \cdot 10^6$ [c14]m^3) represented by this data set, the effective coefficient of friction of rock avalanches [c15]could be considered independent of volume. Consequently, our results suggest that the variation seen in Heim's ratio for these rock avalanches [c16]is not [c17](only) caused by [c18]scale-dependent basal friction, but by differing degrees of fragmentation. This shows that fragmentation plays a governing role in the runout of rock avalanches and should be included in hazard assessments.

4 Conclusions

We studied the dynamics of fragmenting rock avalanches experimentally [c1]to unravel the control of basal friction versus fragmentation on runout [c2]behavior. We find that fragmentation causes both spreading and [c3]frictional interaction - competing processes that control [c4]the avalanche dynamics. Based on energy arguments we derive a scaling law with empirical constants that quantifies the relative importance of [c5]spreading and [c6]frictional interaction as a function of fragmentation. The scaling law approaches an extreme for which runout [c7]is maximized and limited only by basal [c8]friction, which itself might be volume-dependent as suggested by earlier studies. The [c9]scaling law is validated against a natural data set [c10]verifying its [c11]applicability.

Data availability. The data for this paper is available as an open access data publication (Haug et al., 2020).

Video supplement. Videos for this paper is available as an open access data publication (Haug et al., 2020).

[c11]*MRo*: 0.15.
[c12]*MRo*: further
[c13]*MRo*: a
[c14]*MRo*: m^3),
[c15]*MRo*: is
[c16]*MRo*: are
[c17]*MRo*: *Text added.*
[c18]*MRo*: a different
[c1]*MRo*: in order
[c2]*MRo*: behaviour.
[c3]*MRo*: internal friction which compete on the
[c4]*MRo*: of
[c5]*MRo*: spreading, internal
[c6]*MRo*: basal friction
[c7]*MRo*: seems to be dominated
[c8]*MRo*: friction.
[c9]*MRo*: *Text added.*
[c10]*MRo*: proving
[c11]*MRo*: universality and predictive power.

Author contributions. OTH designed and run the experiments, derived the scaling law and wrote the first draft of the manuscript. MRo and MRu assisted in the experiments. MRo, KL and OO were involved in study design. All authors contributed to discussion and writing.

Competing interests. No competing interests are present.

Acknowledgements. The authors would like to thank to Frank Neumann and Thomas Ziegenhagen for construction and technical assistance. The work has been supported by the Helmholtz Graduate Research School GEOSIM, the German Ministry for Education and Research (BMBF, FKZ03G0809A) and the Deutsche Forschungsgemeinschaft (DFG) through grant CRC 1114 “Scaling Cascades in Complex Systems” (No. 235221301) project B01. We thank Kirsten Elger and GFZ Data Services for publishing the data. [c1]We thank the editor Michael Krautblatter and the two anonymous reviewers which provided very helpful comments which improved the manuscript. We thank Jon Bedford for providing a thourough language check of the manuscript.

Appendix A: Definitions

c2

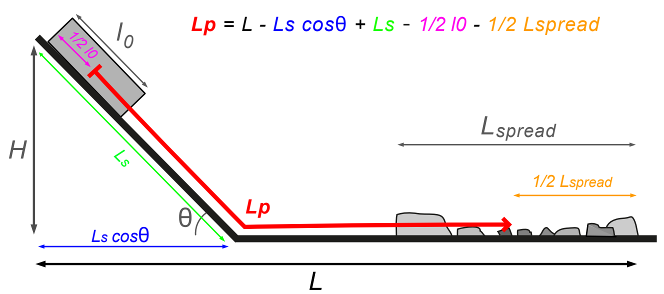

Figure A1. Definition of distances used in Equation 3 . L_p is the length of the travel path.

Appendix B: Scaling law fit to experimental data only

[c1]*MRo: Text added.*
[c2]*MRo: Text added.*

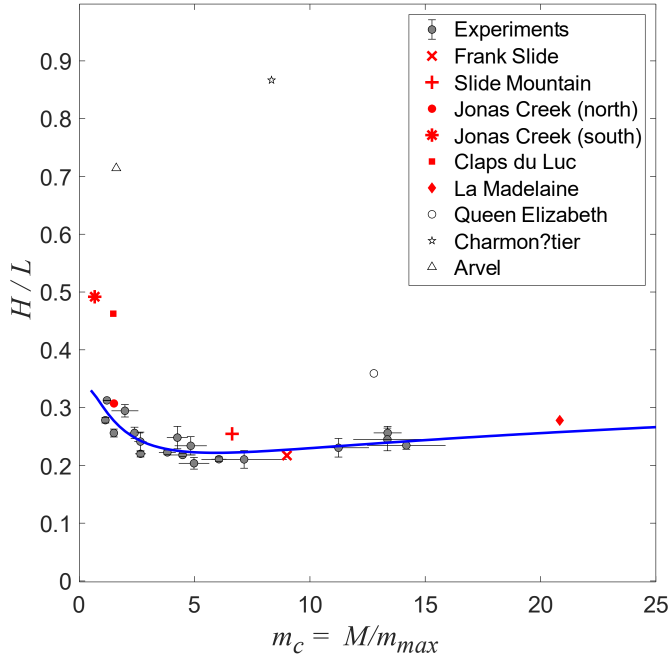

Figure B1. Heim's ratio and deposit length of experiments (this study) and natural rock avalanches (from Locat et al., 2006). The Heim's ratio of the analog experiments (gray) and from the rock avalanches (red = selected set, open = discarded). The blue line represents the best fit of Equation 8 to experimental data with parameters $\alpha = 0.11$, $\beta = 0.68$ and $\gamma = 2.0$. Data shown and a Matlab-script to plot them are available in Haug et al. (2020).

References

Bowman, E. T., Take, W. A., Rait, K. L., and Hann, C.: Physical models of rock avalanche spreading behaviour with dynamic fragmentation, Can. Geotech. J., 49, 460–476, https://doi.org/10.1139/t2012-007, 2012.

Campbell, C. S.: Self-lubrication for long runout landslides, The Journal of Geology, 97, 653–665, http://www.jstor.org/stable/10.2307/30062196, 1989.

Davies, T. R. and McSaveney, M. J.: Runout of dry granular avalanches, Can. Geotech. J., 36, 313–320, https://doi.org/10.1139/t98-108, 1999.

De Blasio, F. V. and Crosta, G. B.: Fragmentation and boosting of rock falls and rock avalanches, Geophysical Research Letters, 42, 8463–8470, https://doi.org/10.1002/2015GL064723, 2015.

Gao, G., Meguid, M. A., Chouinard, L. E., and Zhan, W.: Dynamic disintegration processes accompanying transport of an earthquake-induced landslide, Landslides, pp. 1612–5118, https://doi.org/10.1007/s10346-020-01508-1, https://doi.org/10.1007/s10346-020-01508-1, 2020.

Haug, Ø. T., Rosenau, M., Leever, K., and Oncken, O.: Modelling Fragmentation in Rock Avalanches, Landslide Science for a Safer Geo-Environment, 2, https://doi.org/10.1007/978-3-319-05050-8_16, 2014.

Haug, Ø. T., Rosenau, M., Leever, K., and Oncken, O.: On the Energy Budgets of Fragmenting Rockfalls and Rockslides: Insights from Experiments, Journal of Geophysical Research: Earth Surface, https://doi.org/10.1002/2014JF003406, http://doi.wiley.com/10.1002/2014JF003406, 2016.

Haug, Ø. T., Rosenau, M., Rudolf, M., Leever, K., and Oncken, O.: Laboratory model data from experiments on fragmenting analogue rock avalanches, https://doi.org/http://doi.org/10.5880/GFZ.2020.004, https://dataservices.gfz-potsdam.de/panmetaworks/review/2dfece6228dbb2d7ea320457abfeeb3f5c4a1e76f8a8d48c26ae4d0c7794702f/, 2020.

Heim, A.: Der Bergsturz von Elm., Zeitschrift der Deutschen Geologischen Gesellschaft, pp. 74–115, 1882.

Hsü, K. J.: Catastrophic debris streams (sturzstroms) generated by rockfalls, Geological Society of America Bulletin, 86, 129–140, http://bulletin.geoscienceworld.org/content/86/1/129.short, 1975.

Hungr, O. and Evans, S.: Entrainment of debris in rock avalanches: An analysis of a long run-out mechanism, GSA Bulletin, 116, 1240–1252, https://doi.org/10.1130/B25362.1, https://doi.org/10.1130/B25362.1, 2004.

Hungr, O., Leroueil, S., and Picarelli, L.: The Varnes classification of landslide types, an update, Landslides, 11, 167–194, https://doi.org/10.1007/s10346-013-0436-y, 2013.

Imre, B., Laue, J., and Springman, S. M.: Fractal fragmentation of rocks within sturzstroms: insight derived from physical experiments within the ETH geotechnical drum centrifuge, Granular Matter, 12, 267–285, https://doi.org/10.1007/s10035-009-0163-1, http://link.springer.com/10.1007/s10035-009-0163-1, 2010.

Kent, P. E.: The transport mechanism in catastrophic rock falls, The Journal of Geology, 74, 79–83, http://www.jstor.org/stable/10.2307/30075179, 1966.

Knapp, S. and Krautblatter, M.: Conceptual Framework of Energy Dissipation During Disintegration in Rock Avalanches, Frontiers in Earth Science, 8, 263, https://doi.org/10.3389/feart.2020.00263, https://www.frontiersin.org/article/10.3389/feart.2020.00263, 2020.

Legros, F.: The mobility of long-runout landslides, Engineering Geology, 63, 301–331, http://www.sciencedirect.com/science/article/pii/S0013795201000904, 2002.

Lin, Q., Cheng, Q., Li, K., Xie, Y., and Wang, Y.: Contributions of Rock Mass Structure to the Emplacement of Fragmenting Rockfalls and Rockslides: Insights From Laboratory Experiments, Journal of Geophysical Research: Solid Earth, 125, e2019JB019 296, https://doi.org/10.1029/2019JB019296, https://agupubs.onlinelibrary.wiley.com/doi/abs/10.1029/2019JB019296, e2019JB019296 2019JB019296, 2020.

Locat, P., Couture, R., Leroueil, S., Locat, J., and Jaboyedoff, M.: Fragmentation energy in rock avalanches, Canadian Geotechnical Journal, 43, 830–851, https://doi.org/10.1139/t06-045, 2006.

Lucas, A., Mangeney, A., and Ampuero, J. P.: Frictional velocity-weakening in landslides on Earth and on other planetary bodies., Nature communications, 5, 3417, https://doi.org/10.1038/ncomms4417, http://www.ncbi.nlm.nih.gov/pubmed/24595169, 2014.

Manzella, I. and Labiouse, V.: Empirical and analytical analyses of laboratory granular flows to investigate rock avalanche propagation, Landslides, https://doi.org/10.1007/s10346-011-0313-5, 2012.

Melosh, H. J.: Acoustic Fluidization : A New Geologic Process?, Journal of Geophysical Research, 84, 7513–7520, 1979.

Pudasaini, S. P. and Fischer, J.-T.: A mechanical erosion model for two-phase mass flows, International Journal of Multiphase Flow, 132, 103 416, https://doi.org/https://doi.org/10.1016/j.ijmultiphaseflow.2020.103416, https://www.sciencedirect.com/science/article/pii/S0301932220305255, 2020.

Pudasaini, S. P. and Miller, S. A.: The hypermobility of huge landslides and avalanches, Engineering Geology, 157, 124–132, https://doi.org/https://doi.org/10.1016/j.enggeo.2013.01.012, https://www.sciencedirect.com/science/article/pii/S001379521300032X, 2013.

Shreve, R. L.: Leakage and fluidization in air-layer lubricated avalanches, Geological Society of America Bulletin, 79, 653–658, https://doi.org/10.1130/0016-7606(1968)79, http://bulletin.geoscienceworld.org/content/79/5/653.short, 1968.

Staron, L. and Lajeunesse, E.: Understanding how volume affects the mobility of dry debris flows, Geophys. Res. Lett., 36, 2–5, https://doi.org/10.1029/2009GL038229, http://www.agu.org/pubs/crossref/2009/2009GL038229.shtml, 2009.

Vaunat, J. and Leroueil, S.: Analysis of Post-Failure Slope Movements within the Framework of Hazard and Risk Analysis, Natural Hazards, pp. 83–109, 2002.

Wang, Y. F., Dong, J. J., and Cheng, Q. G.: Velocity-dependent frictional weakening of large rock avalanche basal facies: Implications for rock avalanche hypermobility?, Journal of Geophysical Research: Solid Earth, 122, 1648–1676, https://doi.org/10.1002/2016JB013624, https://agupubs.onlinelibrary.wiley.com/doi/abs/10.1002/2016JB013624, 2017.

Zhao, T., Crosta, G. B., Utili, S., and De Blasio, F. V.: Investigation of rock fragmentation during rockfalls and rock avalanches via 3D DEM analyses, Journal of Geophysical Research: Earth Surface, https://doi.org/10.1002/2016JF004060, http://doi.wiley.com/10.1002/2016JF004060, 2017.

Zhao, T., Crosta, G. B., Dattola, G., and Utili, S.: Dynamic Fragmentation of Jointed Rock Blocks During Rockslide-Avalanches: Insights From Discrete Element Analyses, Journal of Geophysical Research: Solid Earth, 123, 3250–3269, https://doi.org/10.1002/2017JB015210, https://agupubs.onlinelibrary.wiley.com/doi/abs/10.1002/2017JB015210, 2018.